EXPLORING THE PHOTOCATALYTIC ACTIVITY OF DIAMINOMALEONITRILE-DERIVE C=N EXTENDED SYSTEMS: PHOTODEGRADATION OF LYNDANE AS PROOF OF CONCEPT

Antonio López-García,[a] M. Pilar García Armada[c,d], José L. de la Fuente,[b] and Marta Ruiz-Bermejo[a, *]

[a] Centro de Astrobiología (CAB), INTA-CSIC. Dpto. Evolución Molecular. Ctra. Torrejón-Ajalvir, km 4, Torrejón de Ardoz, 28850 Madrid, Spain.

[b] Instituto Nacional de Técnica Aeroespacial "Esteban Terradas" (INTA). Ctra. Torrejón-Ajalvir, km 4, Torrejón de Ardoz, 28850 Madrid, Spain.

[c] Departamento de Ingeniería Química y Medio Ambiente, Escuela Técnica Superior de Ingenieros Industriales, Universidad Politécnica de Madrid, José Gutiérrez Abascal 2, 28006 Madrid, Spain

[d] Nanomateriales 2D Para Aplicaciones en Energía y Sensores, Universidad Politécnica de Madrid, Unidad Asociada al CSIC, José Gutierrez Abascal, 2, 28006 Madrid, Spain

*Corresponding author information: e-mail: ruizbm@cab.inta-csic.es

Telephone: +34 915206458

ABSTRACT

The sustainable development of semiconductive C=N materials, as promising alternative to carbon nitride, needs low-cost, highly efficient and environmental friendly synthetic processes. This topic was achieved through the bulk thermal polymerizations of diaminomaleonitrile (DAMN) or under wet conditions, hydrothermal as well as via *n*-alcohol based on solvothermal methods. Under these premises has been explored the changes in DAMN-based carbon extended conjugated structures with the reaction conditions thought FTIR and solid-state NMR spectroscopies. Complementary characterization methods, such as XRD, EPR and SEM were able to deepen in the effect of the solvent on the DAMN polymers under study. Additionally, their UV-Vis spectra were evaluated, and from these measurements, optical band gap energies around 2.5 eV were estimated. In fact, the semiconducting character of these samples was furthermore supported by electrochemical methods. Their morphological features were also examined. The BET surfaces areas were considerably higher and the size particles were significant lower for the samples synthetized in wet than those synthesized in bulk. Finally, the potential of these 2D-materials for photocatalytic applications was explored. As a result, herein they are described easy one pot synthetic procedures that lead practically quantitative yields in semiconducting and mesoporous materials based on DAMN, using green solvents such as *n*-alcohols at middle temperatures.

Keywords: HCN polymers, DAMN polymers, soft nanoparticles

1. INTRODUCTION

Diaminomaleonitrile (DAMN) present an interesting reactivity due to its symmetric structure with amine and nitrile groups, forming a conjugated system. These DAMN characteristics make it a key molecule in fine synthetic chemistry [Chaudhary 2022], in the production of Schiff base metal complexes [see e.g. Yang et al. 2016, Paul and Barman 2024, Oliveri et al. 2022, Zare et al. 2019] and in the design of colorimetric sensors [see e.g. Ulla et al. 2024, Alharbi et al. 2022, Hanif et al. 2019]. Furthermore, since several years ago, our research focused on using DAMN as a monomer for creating C=N-based highly conjugated extended macrostructures, aiming to develop easy and efficient processes to reach new multifunctional materials with versatile applications (Ruiz-Bermejo et al. 2022, Ruiz-Bermejo et al. 2022b, Ruiz-Bermejo et al. 2019, Hortelano et al. 2024). Thus, the DAMN-derived polymers has emerged as a subject of investigation, encapsulating their fascinating synthesis, optical and electromagnetic characteristic, and multifaceted applications that span the realms of chemistry, physics, and biology.

The thermal induced bulk polymerization of DAMN, in solid state (Mamajanov et al. 2009, Hortelano et al. 2022) as well as in melt (Itziar et al. 2021), achieved high yields, around 90 %, being air-stable (Hortelano et al. 2023) and leading to really reproducible and very fast processes (Ruiz-Bermejo et al. 2024). From these syntheses, it is noteworthy the potential applications of the DAMN polymer obtained in melt (at 190 ºC) such as biosensor (Ruiz-Bermejo et al. 2022) and catalyst (Hortelano et al. 2024). However, the morphology and textural properties of these DAMN-based materials, synthetized in bulk, are not fit. Undefined shape, large size and low specific superficial area were observed for these soft particles. In order to solve these critical trouble, especially important for the design of catalyst or nanomaterials, as well, others syntheses were carried out under hydrothermal conditions assisted by microwave radiation (MWR) (Ruiz-Bermejo et al. 2022), since it is well-known the effect of the solvothermal conditions for the modulation of the morphological and textural properties [Wei et al. 2012 and Taublaender et al. 2019]. The MWR-driven production of DAMN polymers lead to the generation of relative

homogeneous submicron particles, with semiconducting behavior, tough a really fast synthetic method (less than 4 min). However, the yields of these reactions were markedly poor, around 35 %. Thus, as second step, to address the low values conversion of DAMN under hydrothermal conditions but sidestepping the inconvenience of the bulk polymerizations, alcohols were tested as solvents for the self-condensation of DAMN. Practically quantitative yields were attained when 1-pentanol and 1-hexanol were used (López-García et al. 2024).

Based on these previous results, in the present work, the spectroscopic characteristics, the magnetic, optical and electrochemical properties, as well as, the morphological and textural features of several DAMN polymers are comparatively studied in detail. This comprehensive analysis would help to understand how the synthetic conditions have effect on the potential applications as (photo)catalyst of these new promising (but scarcely studied) soft materials. In concrete, four DAMN polymers will be considered for this comparative study: the best accurate DAMN polymer to date, which was synthetized in melt as it was above mentioned (from here to the end of the manuscript it will be referenced as MP-DP), one hydrothermal DAMN polymer synthetized under middle temperatures conditions (WP-DP) and the others two ones obtained using 1-pentanol and 1-hexanol as solvents (PnP-DP and HxP-DP, respectively). Preliminary researches indicated that these four samples present –C=N- extended conjugated macrostructures within resemble features with the extensively studied carbon nitrides [**ref.**].

Thus, taking in mind the use of different carbonitrides for the photocatalytic production of H_2 (Wang et al. 2009, Yang et al. 2017, Florentino-Madiedo et al. 2022, Kong et al. 2023), for the heterogeneous organosynthesis of C-O, C-C, C-N and N-N bonds in photoredox processes (Yang et al. 2017), and the photocatality activity of other HCN-derived polymer (Zhou et al. 2014) (DAMN is the formal tetramer of the HCN), the four DAMN polymers herein considered were tested as potential photocatalyst. As a first and opening approach, the photodegradation of lindane (γ-hexachlorocyclohexane) were monitored. Lindane is a persistent and very toxic pollutant used as broad spectrum insecticide. Currently lindane is banned in most of the countries around the world. However, its presence in surface water and groundwater is still reported (see e.g. An et al. 2023, Brovini et al. 2023, Gandla et al. 2023 and Singh et al. 2023) and the finding of procedures for its photodegradation is an active research topic (Rescigno et al. 2024, Ghaffar et al. 2023, Radic et al. 2022). As main photocatalysts nanoparticles and surfaces

of TiO_2 have been used, in heterocatalytic processes with the additional presence of radical precursors such as H_2O_2 and persulfate ($S_2O_8^{-2}$) and UV or visible light sources (see e.g. Senthilnathan et al. 2009 and 2010 and Khan 2023, 2021, 2019, 2017).

In this way, in the present paper, the DAMN polymers are introduced as potential photocatalyst due to their semiconducting properties and the possibility to modulate their morphological and textural properties by the synthetic conditions.

2. MATERIALS AND METHODS

2.1. Synthetic conditions

The synthetic procedures for the production of the DAMN polymers herein studied were described in detail in López-García et al. 2024. In brief, 135 mg of DAMN were heating in 5 mL of water (WP-DP), 1-pentanol (PnP-DP) or 1-hexanol (HxP-DP) at 90, 130 or 150 ºC, respectively, during 144 h. The final suspensions were filtered and the black solids collected were dried under reduced pressure until a constant weight was reached. Additionally, the DAMN polymer used as reference was synthetized in bulk as follow: 135 mg of DAMN was heating under inert atmosphere (N_2) at 190 ºC during 20 min (MP-DP) (Ruiz-Bermejo et al. 2022). The table 1 summarizes the synthetic conditions used and the yield obtained in each case.

Table 1. Summary of the reaction conditions used in this work for the production of DAMN polymers. The reaction time of 144 h was chosen on the base of the results discussed in (López-García et al. 2024). At shorter reaction times equivalent yields were obtained but at 144h it was proven that the chemical composition of these samples is fixed. The yields [as conversion of DAMN, α (%)] were calculated from the initial amount of DAMN, as follow: α (%) = (135 mg of DAMN/mg of black solid collected)*100. The average values were calculated at least from three independent syntheses.

	Synthetic conditions			**Yield**
Sample	**Solvent**	**T (ºC)**	**T (h)**	**α (%)**
MP-DP	-	190	0.33	88 ± 2
WP-DP	Water	90	144	66 ± 5
PnP-DP	Pentanol	130	144	94 ± 2
HxP-DP	Hexanol	150	144	97 ± 1

2.2. Spectroscopic, morphological and textural characterization

The DAMN polymers were characterized by elemental analysis, FT-IR spectroscopy, ^{13}C nuclear magnetic resonance (^{13}C NMR), X-ray diffraction (DRX), and scanning electron microscopic (SEM), as well as, their density values as it is described in (Ruiz-Bermejo et al. 2022). In addition, the electron spin resonance (ESR) spectra were recorded as it is described in (Pérez-Fernández et al. 2023). The N_2 adsorption isotherms at 77 k….

The UV-vis spectra were recorded by means of a spectrophotometer Agilent 8453, whose working range was from 200 to 750 nm with a resolution of 2 nm, using 1.5 mg of the DAMN polymers dissolved/suspended in 3 mL of different organic solvents and diluting the solutions/suspensions 1:10. In order to compare the different spectra recorded, they were normalized and then smoothed using the Savitzky-Golay algorithm.

2.3. Electrochemical study

The electrochemical study was performed with an Ecochemie BV Autolab PGSTAT 12 with a conventional three-electrode cell at 20–21 ◦C. The working electrode was a Pt disc (3 mm diameter), the auxiliary electrode was a Pt wire, and an Ag/AgCl/KCl 3M electrode (E = 0.22 V vs. SHE) was used as reference electrode. A solution of 0.1 M $NaClO_4$ in dimethyl sulfoxide (DMSO) was used as supporting electrolyte.

2.4.Photodegradation of lindane

Aerosols from suspensions of DAMN polymers (1 mg/mL) in 10 ppm standard solutions of lindane (97%, purchased from Sigma Aldrich, St. Louis, MO, USA, and used as received) in MeOH (HPLC Grade–Merck) were irradiated by UV light using a Spectroline 11SC-1 Hg vapor discharge lamp (254 nm). The solubility of the DAMN polymers in MeOH is negligible and therefore these reactions can be considered as heterogeneous photocatalytic processes. The bubble-aerosol-droplet cycle was established using an ultrasonic aerosol generator (BONECO model 7035). As supplementary information is showed the experimental set-up (video V1).

For the quantification of lindane an Agilent 8860 series gas chromatograph interfaced with an Agilent 5977B GC-MSD mass selective single-axis detector was used. A 1 µL of the methanolic samples, previously centrifuged, was directly injected in splitless mode onto a 30-m DB- 5MS fused-silica column (60 m × 0.25-mm internal diameter and film thickness of 0.25 µm), using the following temperature ramp for the GC: 100 ºC (initial temperature) which was maintained for 1 min, then heated to 260 ºC at 10 ºC/min with a final holding time of 1 min. The injector temperature was 290 ºC. The detector

temperature was 350 ºC. The carrier gas flow was 1.5 mL/min of He. The MS source temperature was 230 ºC and the source was operated at 70 eV. Compound identification was performed in full-scan mode with a range of 50 to 650 amu.

3. RESULTS AND DISCUSSION

This section is organized in three parts. Firstly, a detailed comparative study, taking into account the chemical composition, spectroscopic and thermal characteristics and the morphological and textural properties of the four DAMN polymers chosen. In the second part, the semiconducting behavior of these samples is examined thought their optical and electrochemical properties. And finally, the potential of the DAMN polymers as photocalytist is researched.

3.1. Structural and morphological comparative study

3.1.1. Chemical composition: Elemental analysis

In the **Figure 1a** are showed comparatively the data from the elemental composition of the four samples under study. Interestingly, the sample with a greater amount of nitrogen is MP-DP as well as it is the polymer with a minor content in oxygen, whereas the greater per cent in oxygen is observed in WP-DP. It is important to indicate that this amount of oxygen in MP-DP is related with water absorbed superficially in the macrostructure, from the ambient moisture, due to the hydrophilicity of this polymer, since the reaction was carried out under anhydrous conditions and free of solvents (Ruiz-Bermejo et al. 2022); whereas in PnP-DP and in HxP-DP the presence of oxygen is related with solvent molecules embedded in the polymeric net, forming part of it (crystallization molecules) (López-García et al. 2024). However, in the case of WP-DP the high amount of oxygen can be related with absorbed water but also with structural oxygen in the macrostructure. Due to the especially characteristic of water, it can lead to oxidation and hydrolysis reactions during the polymerization processes and even to secondary co-polymerizations (López-García et al. 2024). Taking into account these considerations, the WP-DP is the sample that it seems to present greater differences respect to the other three ones. No significant compositional variations were observed between PnP-DP and HxP-DP except for the higher oxygen content of HxP-DP, likely due a greater amount of trapped solvent molecules in the macrostructure. Additionally, the molar relationship C/N (**Figure 1b**) is also very informative and give an overview of the notable modifications in the chemical compositions due to the synthetic conditions. Again, whereas between PnP-DP and HexP-

DP are no detected significant variations in the composition of the main polymeric nets based on –C=N- bonds, it is noteworthy the differences found respect to MP-DP and WP-DP where the ratio C/N is significantly lower and absolutely notable in the case of the MP-DP.

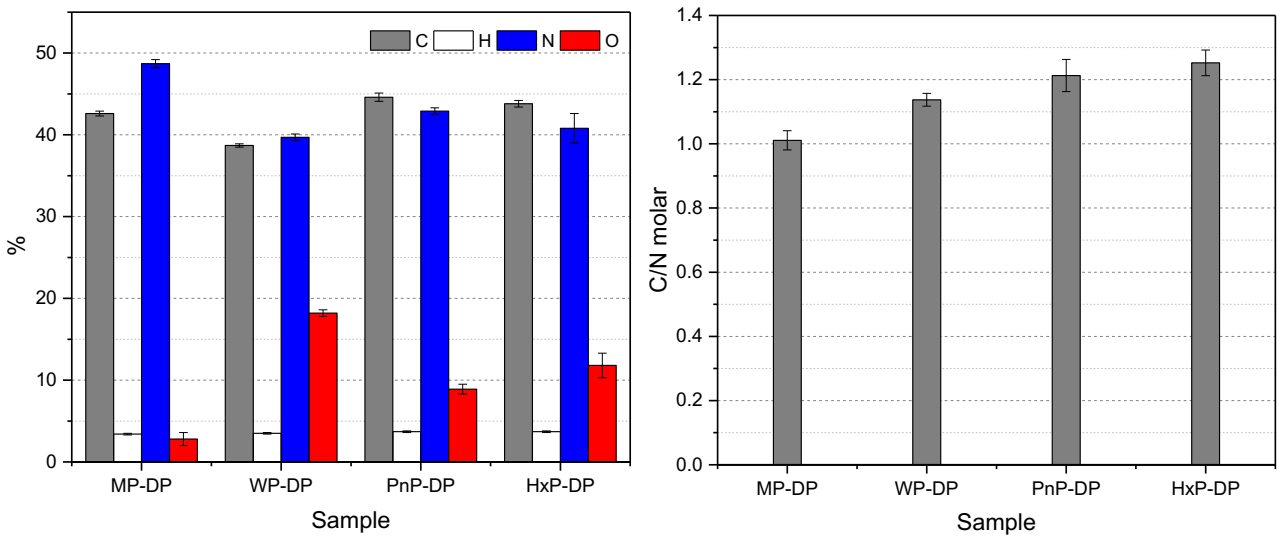

Figure 1. a) Elemental composition of several DAMN polymers, obtained how it is indicated in the **Table 1**; b) Molar relationships C/N of the same DAMN polymers.

3.1.2. Structural spectroscopic analysis

The simultaneous comparative analysis of the FT-IR and ^{13}C NMR spectra of the DAMN polymers herein considered (**Figure 2**) indicates clearly that these polymers present extended C=N-based macrostructures, in strong agreement with the indicated above.

The FT-IR spectra of the four samples present four regions centered about 3300, 2200, 1630 and 700 cm^{-1} (**Figure 2a**), which were discussed in detail elsewhere (Ruiz-Bermejo et al. 2019). Briefly, the three first broad bands are related with functional groups containing nitrogen, such as amines (-NH_2, -NH, ~ 3300 cm^{-1}), nitriles (-C≡N, ~ 2200 cm^{-1}) and imines plus double bonds –C=C- (-C=N- and –C=C-, 1630 cm^{-1}), respectively, and the last feature may be related with **??**.

The ^{13}CNMR spectrum of the WP-DP shows the same profile that analogous samples synthetized under others hydrothermal conditions (Ruiz-Bermejo et al. 2019) (**Figure 2d**), and resonances at 167 ppm, 161-152 ppm, 145-125 ppm and 120-100 ppm were observed. These NMR signals can be related, respectively, with carbon atoms associated to nitrogen but also with oxygen (amide and carboxylic groups, -CONH-, -COO-), with iminic carbons (>C=N-), with double bounds (>C=C<) and finally with cyano functional

groups (-C≡N). The same resonances are observed in the other three polymeric samples except the signal at 167 ppm.

Thus, in order to obtain a better view of the structural differences between all the samples, several spectral subtractions were made. The subtractions of the FT-IR and ^{13}CNMR spectra from the WP-DP and those using *n*-alcohols show that the WP-DP present C=O groups, likely esters and/or amide bonds (from the feature at 1725 cm^{-1} related with C=O stretch in carbonyl compounds and from a resonance at 167 ppm assigned to C=O in ester and amides, deep blue and orange lines in **Figures 2b** and **2e**, respectively). In addition, in agreement with the presence of functional groups containing oxygen in WP-DP, the band at 3565 cm^{-1} is related with –OH bonds (green and orange lines in **Figure 2b**). These results about the observation of spectroscopic fingerprints related with the presence of oxygenated functional groups in the WP-DP sample is in strong agreement with the elemental analysis data commented above. On the other hand, the subtractions of the FT-IR and ^{13}CNMR spectra from the DAMN polymers synthetized using *n*-alcohols reflect that there are no relevant structural differences between them (green lines in **Figure 2b** and **2e**). However, the subtraction profiles of the spectra from the MP-DP and the others ones, mainly indicates that the contribution of the nitrile groups in MP-DP is higher than in the others three DAMN polymers, inferred by the intense band at 2183 cm^{-1} (**Figure 2c**) and by the broad resonance at 145 ppm (**Figure 2f**). Moreover, note that this resonance can also be assigned with C=N heteroaromatic bonds, indicating, likely, a greater conjugation of the macromolecular systems when the DAMN polymers are synthetized in bulk. Finally, point out that the use of no-dried and anhydrous solvents lead to secondary hydrolysis/oxidation processes, as it can be seen by the features at 1725 cm^{-1} in the FT-IR spectra subtractions related to C=O groups (green and red lines, **Figure 2c**) and by the resonances of the ^{13}C NMR spectra subtractions peaks around 165 ppm, green and red lines, **Figure 2f**) which show functional groups related with the incorporation of oxygen in the main structure.

Therefore, all the DAMN polymers considered in this comparative spectroscopic study present a main macrostructure based on a C=N conjugated system. The principal differences found are due to hydrolysis/oxidation processes caused by the synthetic procedures.

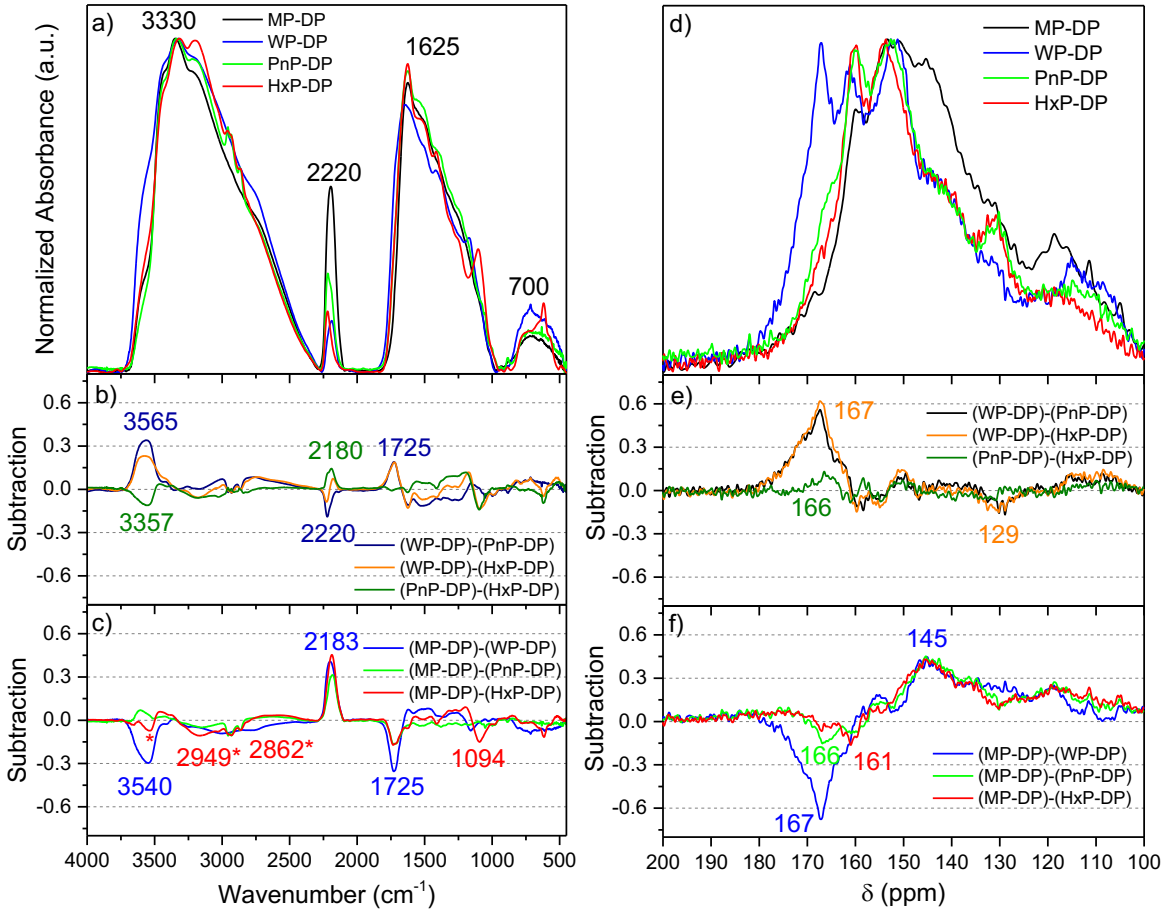

Figure 2. FTIR and ^{13}C NMR Spectra of several DAMN polymers, synthetized as it is indicated in the **Table 1**. a) Normalized FTIR spectra; b) Substractions of the normalized FT-IR spectra, between the DAMN polymer synthetized in water and those prepared using *n*-alcohols; and c) between the DAMN polymer produced by bulk polymerization and those generated by heating using different solvents; d) Normalized ^{13}C NMR spectra, registered in solid state and at room temperature. A scale from 200 to 100 ppm was choose for details. The full spectra from 250 to 0 ppm can be see in (López-García et al. 2024); e) Substractions of normalized ^{13}C NMR spectra, between the DAMN polymer synthetized in water and those prepared using *n*-alcohols; and f) between the DAMN polymer produced by bulk polymerization and those generated by heating using different solvents.

3.1.3. Magnetic and morphological properties

Figure 3a shows the EPR spectra of three representative DAMN polymers. All spectra display a single and symmetric signal center at g = 2.008, which can be related to radicals with only one unpaired electron (S = 1/2) (Delpoux et al. 2011). These results are in strong

agreement with the paramagnetic nature of others HCN-derived polymers (Eastman et al. 2003 + las de Matthews, Pérez-Fernández et al. 2023, Ruiz-Bermejo et al. 2024). Moreover, the paramagnetic behavior of these samples also can explain the broad resonances observed in the NMR spectra discussed above. Qualitatively, the signal intensity of the MP-DP is higher, which would indicate a higher presence of net electronic spin moments in this sample. This behavior may be explain tough the greater π-conjugated C=N based macrostructure of this bulk polymer than the others two ones, as it was discussed for carbon nitrides (Yang et al. 2018), and also may be due to a greater amount of cross-linked structures improving the charge delocalization. Indeed, the intensity of EPR signal decreases with the increasing of the oxygen in the macrostructures, being the EPR signal from the WP-DP the lowest herein observed.

On the other hand, the EPR band symmetry, in turn, could be related to the isotropic nature of these polymers, i.e. their properties do not depend on the direction in which they are measured. Isotropy, at the paramagnetic level, can be present in both amorphous solids and those with spherical particles (Kim et al. 2022). Thus, the symmetry and rearrangement of the samples as well as their morphologies were comparatively analyses by XRD and SEM. The X-ray diffractograms of the DAMN polymeric samples are showed in the **Figure 3b**. All of them show a diffraction centered at 2θ ~ 27º. This single peak, with an interplanar distance around 3.2 Å, for all the cases, is generally related to the (002) diffraction shown by graphitic layered materials (**ref.**). However, it is important to note that any system containing discotic constituents stacked in a nearly planar organisation, or ordered polymeric structures with approximately regular spacing, would also give rise to a similar XRD peak (Miller et al. 2017). Significantly, the XRD patterns of the two DAMN polymers synthetized using *n*-alcohols are practically equal than the diffractograms recorded for formamidium salts derived carbon nitrides (Ciria-Ramos et al. 2019), i.e., these DAMN polymeric samples present amorphous and disordered in-plane and out-of-plane structures, with a nanoscopic rank order only by stacking of the main structure motif, due to the lack of peaks at the bottom of the diffractograms (below 20°). By the contrary, the MP-DP present an additional diffraction at 2θ ~ 13 º that would indicate a more ordered structure. In the particular case of the WP-DP, the same diffraction peaks are observed that those discussed for analogous polymers synthetized at a lower temperature (80 ºC) (Ruiz-Bermejo et al. 2019). Thus, for the WP-DP two different blocks of 2D-structures might be considered. In addition, the crystallinity of

these samples is also specified in the **Figure 3b**, indicating that the HxP-DP sample seems to present the more disordered macrostructure. As a result, the experimental synthetic conditions have a remarkable influence in the arrangements of these DAMN polymers. The use of *n*-alcohols, as solvents, appears to improve the generation of carbonaceous amorphous structures.

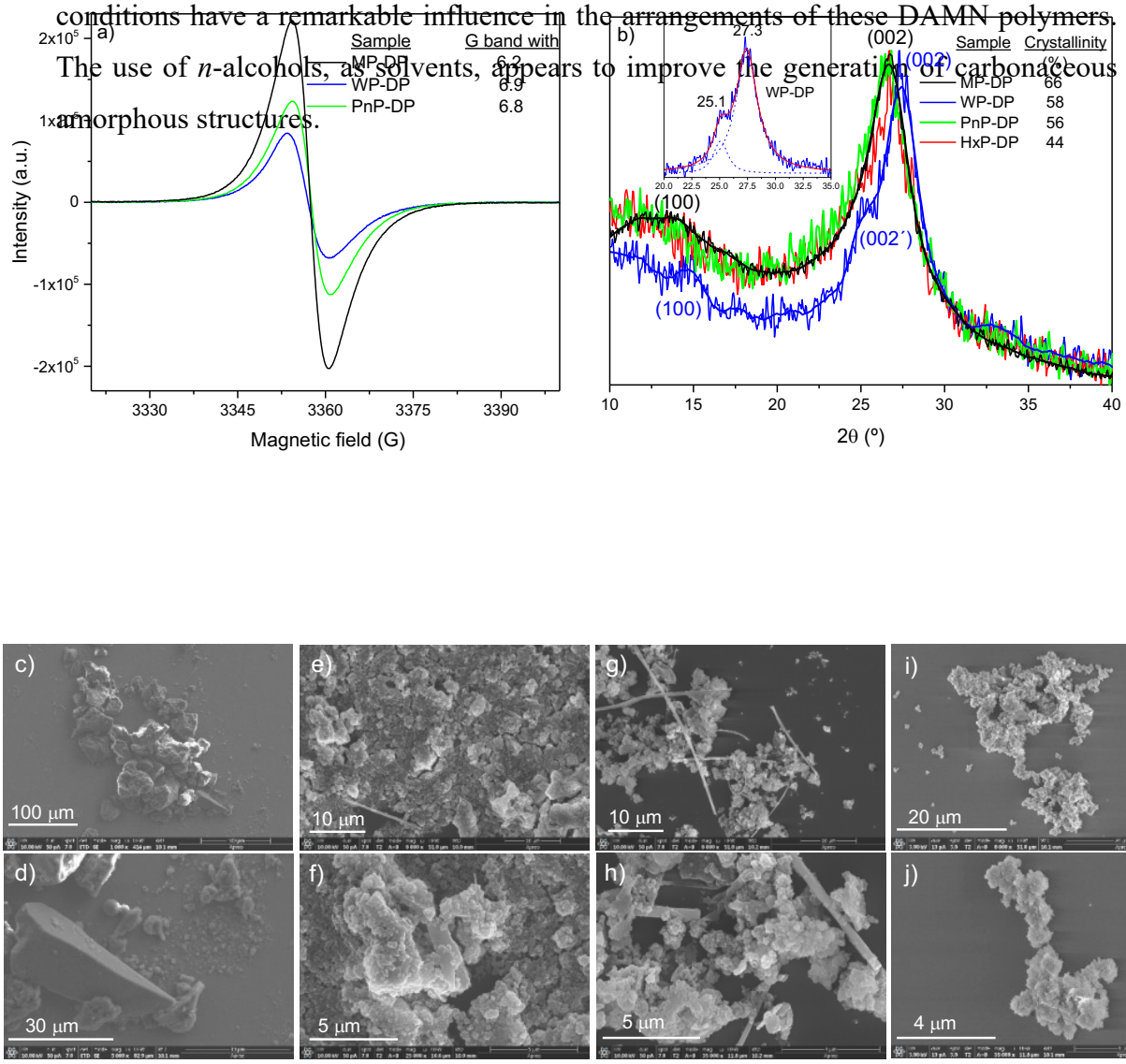

Figure 3. a) EPR spectra of representative DAMN polymers synthetized under different conditions; b) Powder X-ray diffractograms of several DAMN polymers. SEM imagines of the polymeric samples c-d) MP-DP; e-f) WP-DP; g-h) PnP-DP and i-j) HxP-DP.

The SEM imagines (**Figures 3c-j**) show clear differences between the morphologies of the all polymeric samples, in a direct relationship with the synthetic conditions. MP-DP (**Figures 3c-d**) presents irregular and no well-defined shape microparticles whereas in the case of WP-DP several morphologies are observed (**Figures 3e-f**). For this sample, a heterogeneous set of particles are observed: microfibres, laminar structures and sphere-like nanoparticles. A relative morphological resemblance between WP-DP and PnP-DP

is also detected. Again, fibers, laminar microparticles and spherical submicrometric particles are identified in PnP-DP (**Figures 3g-h)**. However, HxP-DP is the most homogeneous sample, only nanospheres are observed (**Figures 3i-j).** Therefore, the solvothermal conditions in the synthetic processes for the production of DAMN polymers modulate clearly the size and shape of the particles obtained.

As summary of this section, one can say that there is no a direct relationship between the paramagnetic properties of the DAMN polymers and their morphological characteristics. In any cases, the DAMN polymers have the capacity to retain stable radicals in their structures, which seems to be related with the C=N conjugation of their macrostructures. Moreover, the heating of DAMN in 1-hexanol lead to the generation of a homogeneous solid constituted by spherical nanoparticles. These are the best synthetic conditions found to date, to the design of potential DAMN-based nanocatalysts, taking into account the morphology of the polymer.

3.1.4. Textural characterization

The morphological differences were also reflected in the textural properties of these DAMN polymers (**Table 2**). As it was expected, the HxP-DP present the highest BET surface area, which is comparable with the values obtained from several carbon nitrides (Florentino-Madievo et al. 2022); whereas WP-DP and Pn-DP show similar values to those previously reported for others hydrothermal DAMN polymers (Ruiz-Bermejo et al. 2022). In any case, the use of solvents for the production of DAMN polymers increasing significantly the BET surface area respect to the DAMN polymers synthetized in bulk.

The N_2 adsorption-desorption isotherms of the solvothermal samples present type-IV isotherm profiles related with mesoporous substances (**Figure 4**).

Table 2. Textural parameters for different DAMN polymers. [a] Data from (Hortelano et al. 2024); * One single point BET surface area, the other three values are from multiple points BET surface area.

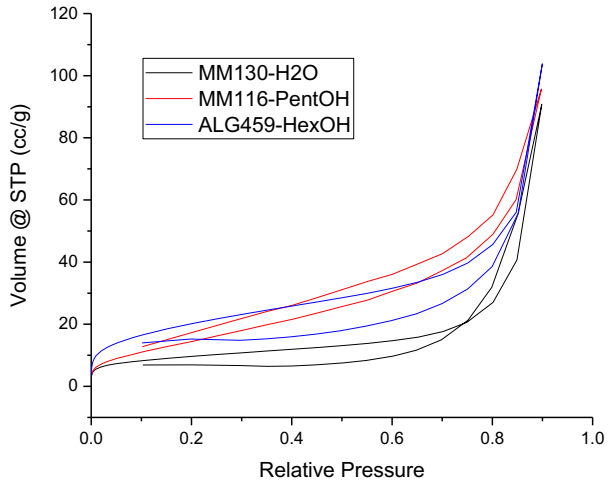

Figure 4. Provisional. La única isoterma que se corresponde con los estándares de material mesoporoso, en esta primera gráfica, es la del PentOH.

3.1.5. Thermal characterization

*The DTG curve profiles for the DAMN polymers here described are very similar to the previously reported for hydrothermal DAMN polymers synthetized at 80 ºC (Ruiz-Bermejo et al. 2019) (compare the Figure 6d of the bibliographic reference with the present **Figure 5a**). After the volatilization of some components of low molecular weight at temperatures below 200 ºC, four main thermal degradation steps are observed (Figure **5a**), in*

Sample	Density (g/cm^3)	S_{BET} (m^2/g)	Total pore volume (cm^3/g)	Peak pore size (nm)
MP-DP	1.64[a]	2.1[a*]		
WP-DP	1.89	30.7		
PnP-DP	1.57	37.3		
HxP-DP	1.58	58.4		

*agreement with the decomposition endothermic peaks showed by the DSC curves (**Figure 5b**). Only a thermal peak observed at ~ 330 ºC in the hydrothermal series at 80 ºC here*

is absence. The lack of this peak might be related with a minor presence of pedant groups in the DAMN polymers here discussed. This result may be due to the higher synthetic temperatures which could improve annelation processes. It is especially significant the resemblance between the DTG profile of the HXP-DP with the DTG curves of the hydrothermal DAMN polymers obtained by assisted microwave radiation) (Ruiz-Bermejo et al. 2022). In fact, in the MP-DP sample only three thermal peak above 200 ºC are observed in its DTG curve (Ruiz-Bermejo et al. 2022b). ESTE TEXTO ES PROVISIONAL.

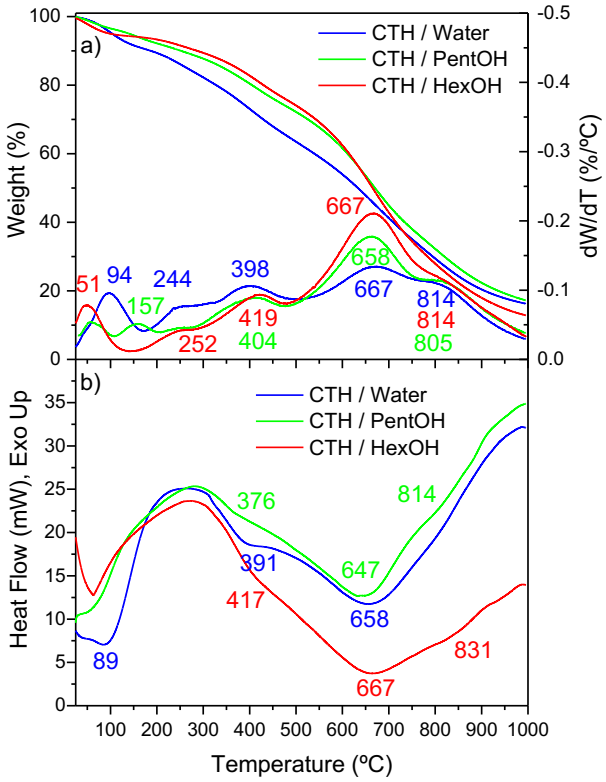

Figure 5. Provisional. Faltan las curvas del MP-DP para que la comparativa sea consistente con el resto de las figuras del trabajo.

3.2. *Semiconducting characteristics*

The semiconducting properties of MP-DP were described and discussed elsewhere (Ruiz-Bermejo et al. 2022 and 2024 and Hortelano et al. 2024). Due to the very low solubility

of this sample, its optical properties were measured by diffuse reflectance spectroscopy (Ruiz-Bermejo et al. 2024) and it is re-dox properties by the modification of solid electrodes (Ruiz-Bermejo et al. 2024). By the contrary, the partial solubility of the WP-DP, PnP-DP and HxP-DP samples in DMSO made possible to record their cyclic voltamograms in solution. Therefore, in this section only the three solvothermal samples will be considered to be study comparatively thought spectroscopic and electrochemical standard measurements in solution.

3.2.1. Optical properties

The UV-vis spectra of the three samples under study were recorded using several solvents with different polarities (**Figure 6**). Note that the cut-off for each solvent is different and therefore the UV-vis spectra were measurement in different wavelength ranges. Also, indicate that the solubility of the DAMN polymers depend on the solvent used and only in some cases their solutions take color. Indeed, these differences in the coloration are clearly observed in the UV-vis spectra, where presumable only a portion of the full sample is able to absorb in the wavelength range considered. Moreover, this heterogeneity in the profile of the UV-vis spectra seems to point out the own heterogeneity of the DAMN polymers. In this sense, it is complex to determinate if these samples present solvatochromism since a no clear and direct shift of the UV-vis absorptions with the polarity of the solvents are observed, despite of the spectral variations showed. However, the three samples display coloration in DMSO and THF. The UV-vis spectra in these solvents present absorbance at ~ 450 nm. Thus, from these spectra were estimated the band gap energy as was previously described for organic semiconductors materials (Costa et al. 2016) (**Figure 7**). The values found around 2.5 eV indicate the semiconductor nature of these DAMN polymers. These optical band gap energies are comparable to several π-conjugated systems such as tetracene (Costa et al. 2016) and numerous carbonitrides (Tian et al. 2023, Fawaz et al. 2023, Junjiang et al. 2014 and Yang et al. 2017). The peaks at ~ 450 nm were also observed in the DAMN polymers synthetized using microwave radiation (Ruiz-Bermejo et al. 2022b) and in carbonitrides (Yang et al. 2017). This absorbance can be related con π-π* transitions along the polymeric networks (Yamamoto et al. 2002). In addition, the absorptions at ~ 330 nm, ~ 260 nm, ~ 230 and ~ 210 nm can be assigned to aromatic fragments (Wait et al. 1966) and π-extended conjugated systems on N-heterocycles macromolecular chains (Toba et al. 2009), to N-heterocycles such as pyrimidines, to lactams and amides and α,β-unsaturated nitriles, and to conjugated bonds

such as –C=C- and –C=C-C=N-, respectively. Therefore, despite of the partial solubility of the DAMN polymers, the UV-vis spectra showed in the **Figure 6** allow to corroborate that these substances are really high conjugated systems with semiconductive properties. However, the optical band gap energies for the solvothermal samples are really higher than that obtained for the MP-DP (0.76 eV) (Ruiz-Bermejo et al. 2024).

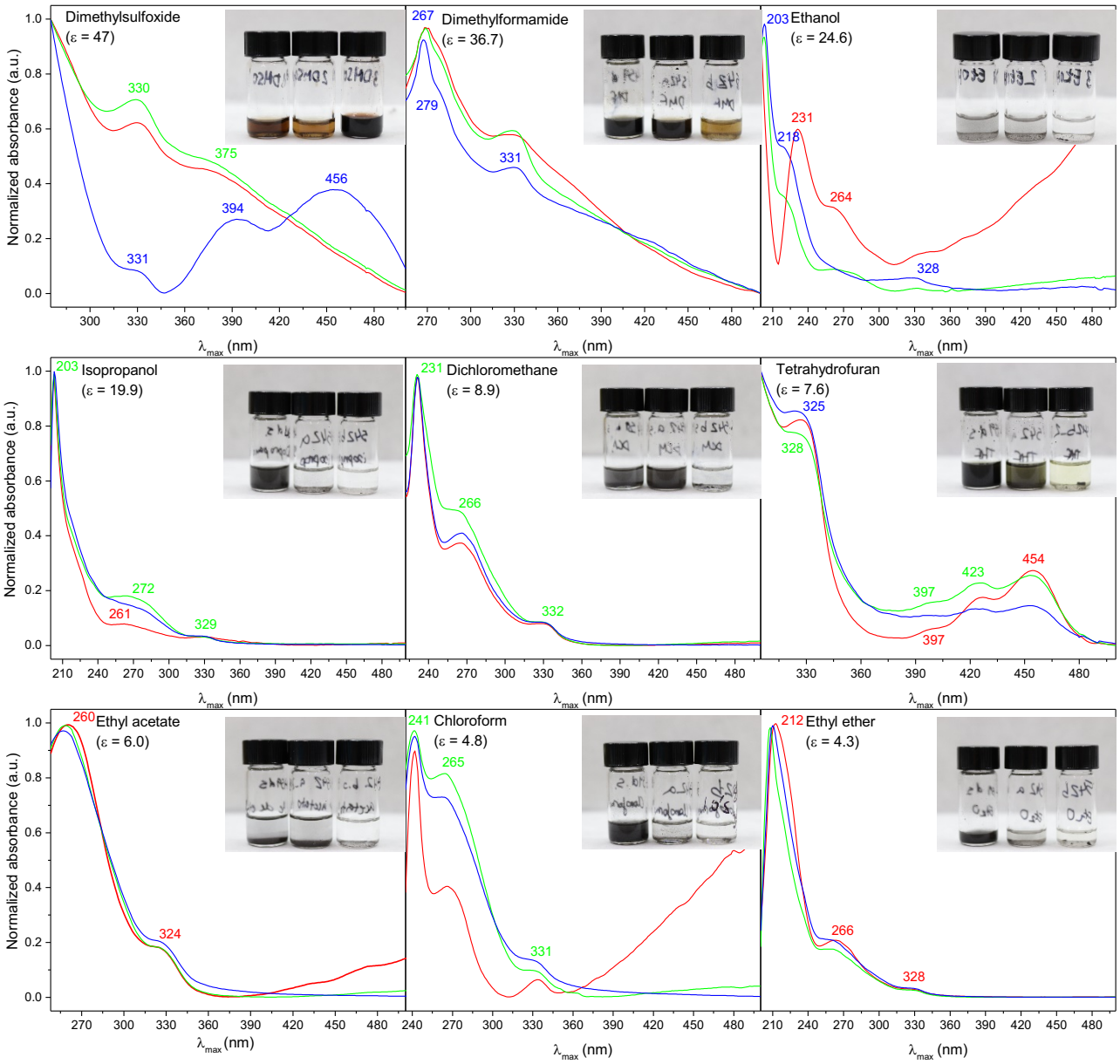

Figure 6. Normalized UV-vis spectra of DAMN polymers in the indicated solvents. ε = dielectric constant of the solvent. In blue lines WP-DP; in green lines PnP-DP; and in red lines HxP-DP. In the insert photographs: solutions/suspensions of DAMN polymers (1.5 mg of polymer/3 mL of solvent). From left to right for each images: HxP-DP, PnP-DP and WP-DP. In order to record the UV-vis spectra, the solutions/suspensions were centrifuged before the measurement.

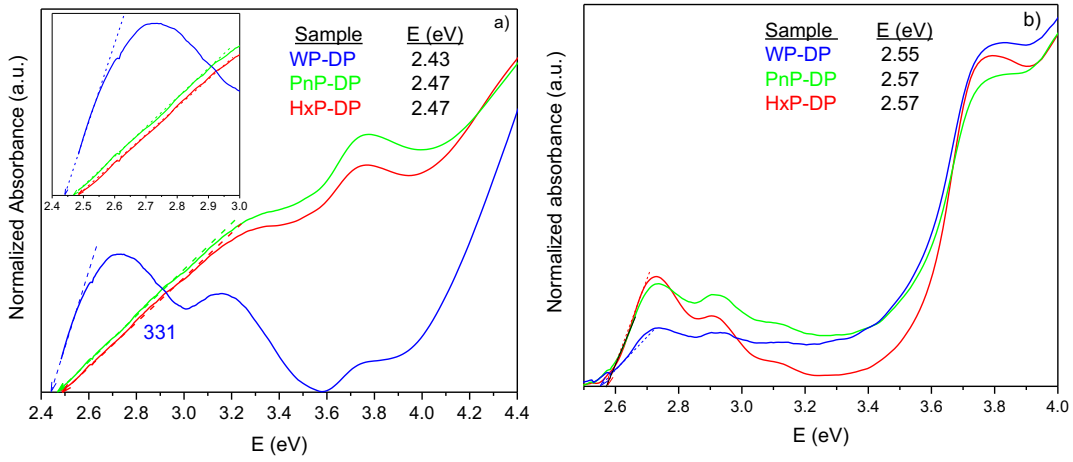

Figura 7. Estimation of the opti**cal band g**ap energy of several DAMN polymers dissolved in a) DMSO and b) THF.

3.2.2. Electrochemical study

With the purpose of complete the characterization of these new DAMN polymers, their electrochemical behaviour has been studied. Figure 8 shows the cyclic voltammograms (CV) obtained from DMSO solutions (about 0.1 g L^{-1}) of WP-DP, PnP-DP and HxP-DP polymers. As it can be seen, the polymer obtained in water show different CV to those obtained in non-aqueous media. The WP-DP polymer presents two redox systems well defined, one reversible system around 0.7 V, and other quasi-reversible around -0.7 V. The PnP-DP and HxP-DP also show two systems, but poorly defined. Furthermore, unlike the WP-DP polymer, the system that now appears around 0.5 V is irreversible.

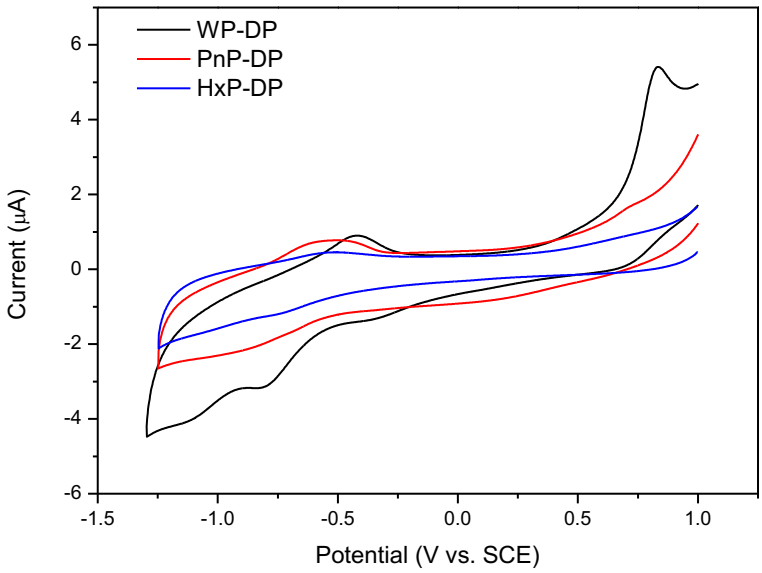

Figure 8. Cyclic voltammogram of DAMN polymers in 0.1 M NaClO4/DMSO. Scan rate 100 mV s-1.

The formal potentials, as well as the onset of peaks, calculated from the voltammograms, also can be used to estimate the highest occupied molecular orbital (HOMO), the lowest unoccupied molecular orbital (LUMO), and the band gap (gap between the HOMO and the LUMO) (Admassie et al.2006) (Johansson et al. 2003). The formal potentials are calculated as the average of the anodic and cathodic peak potentials and the onset values usually are estimated by the intersection between the tangent line drawn to the rising current and the baseline. For all these calculations, the values of the absolute potential for the standard hydrogen electrode (SHE) and the potential difference between the Ag/AgCl and SHE of 4.43 eV and 0.22 V were used. Table 3 shows the results obtained by both methods.
As it can be seen, all the polymers showed similar Eg values, with a somewhat higher average value of 1.38 eV for the WP-DP polymer, and very similar values of 1.22 eV and 1.20 eV for the PnP-DP and HxP-DP polymers, respectively. Nothe than in all cases, the Eg values were higher than CON CUAL HAY QUE COMPARAR?

Table 3. Electrochemical data obtained from the peak potential and from the onset values

Sample	E^0_{ox} (V)	E^0_{red} (V)	HOMO (eV)	LUMO (eV)	Eg (eV)	E_{on}^{ox} (V)	E_{on}^{red} (V)	HOMO (eV)	LUMO (eV)	Eg (eV)
WP-DP	0.76	-0.61	5.41	4.04	1.37	0.75	-0.65	5.40	4.00	1.40
PnP-DP	0.72	-0.46	5.37	4.19	1.18	0.65	-0.61	5.30	4.04	1.26
HxP-DP	0.59	-0.64	5.24	4.01	1.23	0.54	-0.63	5.19	4.02	1.17

3.3. Potential application in photocatalysis. First assay: photodegradation of lindane

Herein, standard methanol solutions of lindane were prepared. These one were irradiated using UV-light during 24 h in the presence of the four DAMN polymers. A clear diminution of the chromatographic peak of lindane were observed (**Figure 9**). Although in any case the photodegradation of lindane was full, all DAMN polymers showed catalytic activity and their effectiveness as photocatalysts was really different. This fact is totally points out when the kinetic of the processes is monitored as was previously reported by Senthilnathan et al. 2009 and 2010. In the **Figure 10a** is showed the relationship C_0/C (C and C_0 are the concentration of lindane at time "t" and at time = 0, respectively). For photodegradation experiments using TiO_2 a modified Langmuir-Hinshelwood kinetic equation was used, $\ln[C_0/C] = kt$, being k a pseudo-first order rate

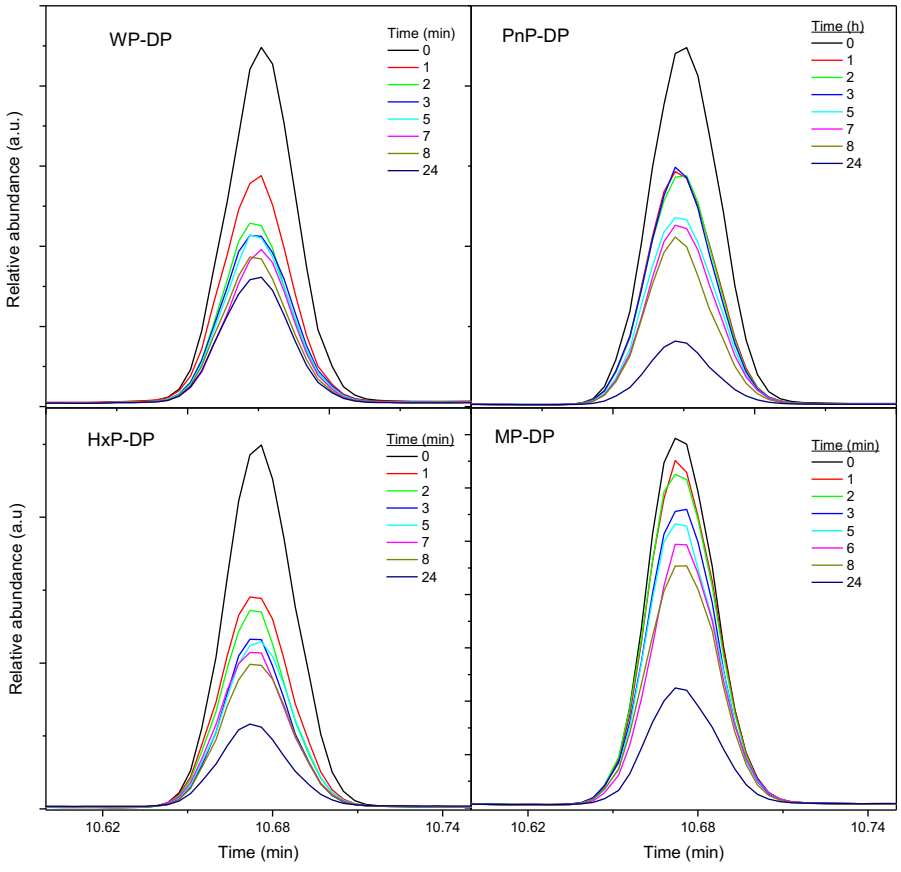

Figure 9. GC-MS chromatograms showing the photodegration of lindane in presence of several DAMN polymers. Note that for clarity in the interpretation of the data, only it is showed the retention time interval where the chromatophic peak of lindane is detected.

constant. In the present case, the use of this expression seems to be only useful to describe properly the kinetic for the sample MP-DP taking into account the clear lineal decreasing

of the lindane concentration against time and the values of the R^2 calculated for a linear fit with a reaction rate of 0.047 h^{-1} (**Figure 10b**). On the other hand, although for the polymer HxP-DP a good R^2 is found for a linear fit (**Figure 10b**), it is evident that the kinetic of this process cannot be adequately adjusted to a first order reaction since in the first hour of reaction a sudden reduction of the lindane concentration is observed (**Figure 9c, Figure 10a**). The same effect is observed for the other two polymers, WP-DP and PnP-DP (**Figures 9 and 10a**). However, after eight hours, no photocatalytic effect is observed for the WP-DP sample, since the C/C_0 seems to remain constant, but the best catalyst appears to be the PnP-DP with a photodegradation of lindane from 10 ppm to 1.7 ppm.

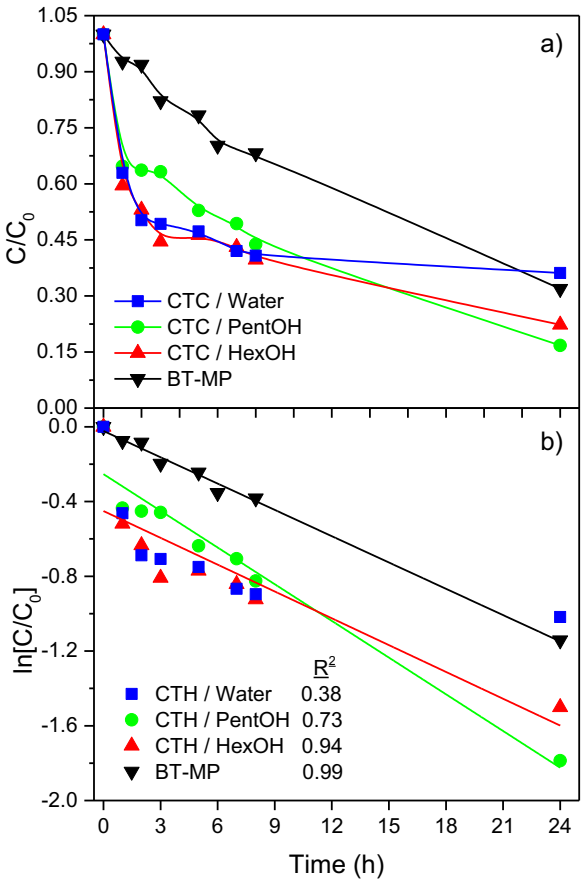

Figure 10. a) Effect of the UV light-activate DAMN polymers photocatalysis of lyndane. $[Lindane]_0$ = 10 ppm in MeOH. The DAMN polymers were suspended in aerosols from lindane solutions in MeOH; b) Approach to a first order kinetic for the photodegradation of lindane using DAMN polymers as catalysts. The lindane only in presence of UV light (wavelength 254 nm) does not undergo photodegradation (Khan et al. 2021 and 2017b).

Note that the main goal of the present study is show the solvothermal effect in the properties of the DAMN polymers obtained. At this moment, no develop efficient and useful photocatalyzers. Thus, as key point, it is important to underline that for the first time the photocatalytic activity of the DAMN polymers has been demonstrated univocally. Herein, no optimal conditions were used for the total degradation of lindane such as the presence of radical precursors but the results here discussed are really useful as starting point for further improvement. Highlight that the use of *n*-alcohols as solvents for the production of DAMN polymers increases very significantly their surface area and the same time leads to solids with lower density. These properties may be the responsible of the better catalytic activity observed for the PnP-DP and HxP-DP samples under the specific conditions herein assayed. In any case, it is demonstrated that synthetic conditions have a significant impact on the catalytic properties of DAMN polymers.

4. CONCLUSIONS AND OUTLOOKS

In order to reach effective and high yield web syntheses of DAMN polymers are necessary a thermal activation of the system and polar protic solvents. In this sense, *n*-alcohols, such as *n*-pentanol and *n*-hexanol, have been shown as excellent solvents for the DAMN polymerization, leading to the production of paramagnetic C=N conjugated macrostructures, with semiconductive properties and relative high surface areas. This characteristic have revealed the potential of the DAMN polymers for the development of a new class of photocatalyzers.

From the starting point herein showed, and the good results in the modification of the HCN-derived polymers using microwave assisted reactions (Hortal et al. 2020), further works are in progress to obtain new DAMN polymers from this methodologies using alcohols are solvents.

Acknowledgements

The authors used the research facilities of the Centro de Astrobiología (CAB) and the Instituto Nacional de Técnica Aeroespacial “Esteban Terradas” (INTA). This research has been funded by grant No. PID2022-140180OB-C22 by the Spanish Ministry of

Science and Innovation/State Agency of Research MCIN/AEI/ 10.13039/501100011033 and by “ERDF A way of making Europe”. A.L.-G.. wants to express his gratitude to INTA for his predoctoral contract. Additionally, the authors are grateful to the M. Teresa Fernández for performing the XRD measurements, to the Service of Electronic Spin Resonance of the Centro de Ayuda a la Investigación of the Universidad Complutense of Madrid (UCM), to the Services of Thermal Analysis and Chemical Analysis of the Instituto de Ciencias de Materiales de Madrid (ICMM, CSIC) and also to Pilar Valles for her support in the SEM analysis.

References

Admassie, S.; Inganäs, O.; Mammo, W.; Perzon, E.; Andersson, M.R. Electrochemical and optical studies of the band gaps of alternating polyfluorene copolymers. Synth. Met. 2006, 156, 614–623, https://doi.org/10.1016/j.synthmet.2006.02.013.

Alharbi, K. H. A Review on Organic Colorimetric and Fluorescent Chemosensors for the Detection of Zn(II) Ions. Critical Reviews in Analytical Chemistry **2022**, DOI10.1080/10408347.2022.2033611.

Rui An, Bin Li, Sining Zhong, Guyu Peng, Jie Li, Ruoqi Ma, Qian Chen, Jinren Ni. Distribution, source identification, and health risk of emerging organic contaminants in groundwater of Xiong'an New Area, Northern China. Science of the Total Environment 893 (**2023**) 164786.

Aruna, Bhawna Rani, Suman Swami, Arunava Agarwala, Debasis Behera. Recent progress in development of 2,3-diaminomaleonitrile (DAMN) based chemosensors for sensing of ionic and reactive oxygen species. RSC Adv., **2019**, 9, 30599–30614.

Bruno Mattia Bizzarri, Angelica Fanelli, Silvia Cesarini, and Raffaele Saladino. A Three-Way Regioselective Synthesis of Amino Acid Decorated Imidazole, Purine and Pyrimidine Derivatives by Multicomponent Chemistry Starting from Prebiotic Diaminomaleonitrile. Eur. J. Org.Chem. **2022**, e202200598.

Emília Marques Brovini, Gabrielle Rabelo Quadra, José R. Paranaíba, Luana Carvalho, Renata de Oliveira Pereira, Sergio Francisco de Aquino. Occurrence and environmental risk assessment of 22 pesticides in Brazilian freshwaters. Aquatic Toxicology 260 (**2023**) 106566.

R. Begland, D. Hartter, F. Jones, D. Sam, W. Sheppard, O. Webster y F. Weigert. Hydrogen Cyanide Chemistry. VIII. New Chemistry of Diaminomaleonitrile. Heterocyclic Synthesis. Journal of Organic Chemistry, vol. 39, nº 16, pp. 2341-2350, **1974**.

Chaudhary, A. 2,3-Diaminomaleonitrile: A Multifaceted Synthon in Organic Synthesis. Current Organic Synthesis **2022**, 19, 616-642

Ciria-Ramos, I., Navascués, N., Diaw, F., Furgeaud, C., Arenal, R., Ansón-Casaos, A.,

& Juarez-Perez, E. J. (**2022**). Formamidinium halide salts as precursors of carbon nitrides. Carbon.

Johansson, T.; Mammo, W.; Svensson, M.; Andersson, M.R.; Inganäs, O. Electrochemical bandgaps of substituted polythiophenes. J. Mater. Chem. 2003, 13, 1316–1323, https://doi.org/10.1039/B301403G.

Jose C.S. Costa, Ricardo J.S. Taveira, Carlos F.R.A.C. Lima, Adelio Mendes, Luís M.N.B.F. Santos. Optical band gaps of organic semiconductor materials. Optical materials **2016**, 58, 51-60.

Dalton, S.; Heatley, F.; Budd, P.M. Thermal Stabilization of Polyacrylonitrile Fibres. Polymer **1999**, 40, 5531–5543.

Aastha Dua, Pravinkumar Selvam, S. Abdul Majeed, S.K. Ashok Kumar, Harish K. Sharma, Selva Kumar Ramasamy. Diaminomaleonitrile Schiff base with phenothiazine aldehyde as multimode chemosensor for copper ions and its application. Journal of Photochemistry & Photobiology, A: Chemistry 447 (**2024**) 115219.

O. Delpoux, D. Gourier, H. Vezin, L. Binet, S. Derenne and F. Robert, *Geochim. Cosmochim. Acta*, **2011**, 75, 326–336.

M. Fawaz, R. Bahadur, N.P. Dharmarajan, J.H. Yang, C.I. Sathish, A.M. Sadanandan, V. Perumalsamy, G. Singh, X. Guan, P. Kumar, A. Vinu, Emerging trends of carbon nitrides and their hybrids for photo-/electro-chemical energy applications, Carbon 214 (**2023**) 118345.

Ferris, J.P.; Hagan, W.J., Jr. HCN and Chemical Evolution: The Possible Role of Cyano Compounds in Prebiotic Synthesis. Tetrahedron **1984**, 40, 1093–1120.

L. Florentino-Madiedo, E. Díaz-Faes, C. Barriocanal. Relationship between gCN structure and photocatalytic water splitting efficiency. Carbon **2022**, 187, 462-476.

Vamshi Krishna Gandla, Mounika Chiluka, Harish Gupta, Sukesh Narayan Sinha, Paromita Chakraborty. Sediment-water partitioning and risk assessment of organochlorine pesticides along the urban, peri-urban and rural transects of Krishna River Basin, Peninsular India. Science of the Total Environment 874 (**2023**) 162360.

Abdul Ghaffar, Tabata Masaaki, Rukhsanda Aziz, Saima Sarfraz. Catalytic degradation of lindane using gamma radiations: Degradation products. Radiation Physics and Chemistry 205 (**2023**) 110741.

Caroline Grundke, Caleb Kong, Christopher J. Kampf, B. Frank Gupton, D. Tyler McQuade, Till Opatz. Programmed Formation of HCN Oligomers through Organosulfur

Catalysis. J. Org. Chem. **2021**, 86, 10320−10329.

V.P. Gupta, Poonam Rawat, R.N. Singh, Poonam Tandon. Formation of 2-imino-malononitrile and diaminomaleonitrile in nitrile rich environments: A quantum chemical study. Computational and Theoretical Chemistry 983 (**2012**) 7–15.

Hanif, M; Rafiq, M; Mustaqeem, M; Shaheen, MA; Qadri, KFI; Qadri, I; Saleem, M. Intracellular and Extracellular Zinc Detection by Organic Fluorescent Receptor. Current Org. Chem. **2019**, 23, 2664-2678.

G. Henrici-Olive´, S. Olive´, in: H.J. Cantow, G. Dall'Asta (Eds.), Advances in Polymer Science, vol. 32, Springer, Berlin, **1979**, p. 123.

Hortelano, C.; Ruiz-Bermejo, M.; de la Fuente, J. L. Solid-state polymerization of diaminomaleonitrile: toward a new generation of conjugated functional materials. Polymer **2021**, 223, 123696.

Hortelano, C., Ruiz-Bermejo, M. & de la Fuente, J.L. Thermal behavior and decomposition mechanism of ammonium perchlorate in the presence of C–N conjugated polymers based on diaminomaleonitrile. J Therm Anal Calorim (**2024**). https://doi.org/10.1007/s10973-023-12871-1

Z. Junjiang, X. Ping, L. Hailong, S.A.C. Carabineiro, Graphitic carbon nitride: synthesis, properties, and applications in catalysis, ACS Appl. Mater. Interfaces 6 (**2014**) 16449-16465.

Sanaullah Khan, Javed Ali Khan, Noor S. Shah, Murtaza Sayed, Muhammad Ateeq, Sabah Ansar, Grzegorz Boczkaj and Umar Farooq. Determination of lindane in surface water samples and its degradation by hydrogen peroxide and persulfate assisted TiO_2-based photocatalysis. RSC Adv., **2023**, 13, 20430.

S. Khan, M. Sohail, C. Han, J. A. Khan, H. M. Khan and D. D. Dionysiou, Degradation of highly chlorinated pesticide, lindane, in water using UV/persulfate: Kinetics and mechanism, toxicity evaluation, and synergism by H_2O_2. J. Hazard. Mater. **2021**, 402, 123558.

S. Khan, C. Han, M. Sayed, M. Sohail, S. Jan, S. Sultana, H. M. Khan and D. D. Dionysiou, Exhaustive photocatalytic lindane degradation by combined simulated solar lightactivated nanocrystalline TiO_2 and inorganic oxidants. Catalysts, **2019**, 9, 425.

S. Khan, C. Han, H. M. Khan, D. L. Boccelli, M. N. Nadagouda and D. D. Dionysiou, Efficient degradation of lindane by visible and simulated solar lightassisted S-TiO_2/peroxymonosulfate process: kinetics and mechanistic investigations, Mol. Catal., **2017**, 428, 9–16.

Sanaullah Khan, Xuexiang He, Javed Ali Khan, Hasan M. Khan, Dominic L. Boccelli, Dionysios D. Dionysiou. Kinetics and mechanism of sulfate radical- and hydroxyl radical-induced degradation of highly chlorinated pesticide lindane in UV/peroxymonosulfate system. Chemical Engineering Journal 318 (**2017b**) 135–142.

Kim, Y., & Zhao, X. (**2022**). Magnetic soft materials and robots. *Chemical Reviews*, 122(5), 5317-5364.

Kito, N., & Ohno, A. (**1974**). Synthesis and reactions of N, N'-dichlorodiiminosuccinonitrile. *The Journal of Organic Chemistry*, 39, 3373-3375.

Klemens Koch, W. Bernd Schweizer, and Albert Eschenmoser. Reactions of the HCN-Tetramer with Aldehydes. Chem. Biodiver. 2007, 4, 541-443.

Kong, X.; Yang, F.; Li, X.; Fu, M.; Zeng, T.; Song, S.; He, Z.; Yu, Y. Covalent Triazine Frameworks Decorated with Pyridine-Type Carbonitride Moieties: Enhanced Photocatalytic Hydrogen Evolution by Improved Charge Separation. Polymers **2023**, 15, 1781.

Miller, T. S., Jorge, A. B., Suter, T. M., Sella, A., Corà, F., & McMillan, P. F. (**2017**). Carbon nitrides: synthesis and characterization of a new class of functional materials. *Physical Chemistry Chemical Physics*, 19(24), 15613-15638.

Mamajanov, I.; Herzfeld, J. HCN Polymers Characterized by SSNMR: Solid State Reaction of Crystalline Tetramer (Diaminomaleonitrile). J. Chem. Phys. **2009**, 130, 134504.

Mas, I.; Hortelano, C.; Ruiz-Bermejo, M.; de la Fuente, J. L. Highly efficient melt polymerization of diaminomaleonitrile. Eur. Polym. J. **2021**, 143, 110185.

Oliveri, IP; Consiglio, G; Munzi, G; Failla, S; Di Bella, S. Deaggregation properties and transmetalation studies of a zinc (II) salen-type Schiff-base complex. Dalton Transactions **2022**, 51, 11859-11867.

Paul, S; Barman, P. Exploring diaminomaleonitrile-derived Schiff base ligand and its complexes: Synthesis, characterization, computational insights, biological assessment, and molecular docking. J. Mol. Struc. **2024**, 1296, 136941.

Pérez-Fernández, C.; Vega, J.; de la Fuente, J. L.; Mateo-Martí, E.; Valles, P.; Ruiz-Bermejo, M. Ammonium affects the wet chemical network of HCN: Feedback between prebiotic chemistry and materials science. Phys. Chem. Chem. Phys. **2023**, 25, 20473.

Nenad Radic , Bosko Grbic, Stevan Stojadinovic, Mila Ilic, Ognjen Dosen, and Plamen Stefanov. TiO_2–CeO_2 composite coatings for photocatalytic degradation of chloropesticide and organic dye. J Mater Sci: Mater Electron (**2022**) 33:5073–5086.

Raffaella Rescigno, Olga Sacco, Stefania Pragliola, Luisa Albarano, Giovanni Libralato, Giusy Lofrano, Vincenzo Romano Spica, Olimpia Tammaro, Giorgia Montalbano, Serena Esposito, Vincenzo Vaiano, Vincenzo Venditto. Environmentally safe ZVI/ZnS-based polymer composite for lindane degradation in water: Assessment of photocatalytic activity and eco-toxicity. Separation and Purification Technology 330 (**2024**) 125246.

Ruiz-Bermejo, M.; García-Armada, P.; Valles, P.; de la Fuente, J. L. Semiconducting soft submicron particles from the microwave-driven polymerization of diaminomaleonitrile. Polymers **2022**, 14, 3460.

Ruiz-Bermejo, M.; García-Armada, P.; Mateo-Martí, E.; de la Fuente, J. L. HCN-derived polymers from thermally induced polymerization of diaminomaleonitrile: A non-enzymatic peroxide sensor based on prebiotic chemistry. Eur. Polym. J. **2022b**, 162, 110897.

Ruiz-Bermejo, M.; de la Fuente, J. L.; Carretero-González, J.; Luis García-Fernández, L.; Aguilar, M. R. A comparative study of HCN polymers synthesized from NH_4CN or DAMN polymerization in aqueous media: New perspectives for prebiotic chemistry and materials science. Chem. Eur. J. **2019**, 25, 11437-11455.

Hilda Sandström and Martin Rahm. Crossroads at the Origin of Prebiotic Chemical Complexity: Hydrogen Cyanide Product Diversification. J. Phys. Chem. A **2023**, 127, 4503−4510.

Sánchez-Soto, P. J., Avilés, M. A., Del Rıo, J. C., Ginés, J. M., Pascual, J., & Pérez-Rodrıguez, J. L. (**2001**). Thermal study of the effect of several solvents on polymerization

of acrylonitrile and their subsequent pyrolysis. *Journal of Analytical and Applied Pyrolysis*, 58, 155-172.

Sandeep Singh, Meenakshi Rawat, Sandeep K. Malyan, Rajesh Singh, Vinay Kumar Tyagi, Kaptan Singh, Sujata Kashyap, Sumant Kumarf, Manish Sharma, B.K. Panday, R.P. Pandey. Global distribution of pesticides in freshwater resources and their remediation approaches. Environmental Research 225 (**2023**) 115605.

Senthilnathan, J., Philip, L., **2010**. Photocatalytic degradation of lindane under UV and visible light using N-doped TiO_2. Chemical engineering journal 161, 83–92.

Senthilnathan, J., Philip, L., Removal of mixed pesticides from drinking water system by photodegradation using suspended and immobilized TiO_2. Journal of Environmental Science and Health Part B (**2009**) 44, 262–270.

M. Josef Taublaender, Manuel Reiter, and Miriam M. Unterlass. Highly Crystalline, Nanostructured Polyimide Microparticles viaGreen and Tunable Solvothermal Polymerization. Macromolecules **2019**, 52, 6318−6329.

Thissen, H.; Koegler, A.; Salwiczek, M.; Easton, C.D.; Qu, Y.; Lithgow, T.; Evans, R.A. Prebiotic-Chemistry Inspired Polymer Coatings for Biomedical and Material Science Applications. NPG Asia Mater. **2015**, 7, e225.

B. Tian, D. Ho, J. Qin, J. Hu, Z. Chen, D. Voiry, Q. Wang, Z. Zeng, Framework structure engineering of polymeric carbon nitrides and its recent applications, Prog. Mater. Sci. 133 (**2023**) 101056.

Ullah, Z; Subramanian, S; Lim, H; Dogan, NA; Lee, JS; Nguyen, TS; Yavuz, CT. Highly Selective and Scalable Molecular Fluoride Sensor for Naked-Eye Detection. ACS App. Mat. Interf. **2024**, DOI10.1021/acsami.4c01187.

Wait, S.C.;Wesley, J.W. Azanaphthalenes: Part I. Huckel orbital calculations. *J. Mol. Spectrosc.* **1966**, 19, 25–33.

Wang, X. et al. J. Am. Chem. Soc. **2009**, 131, 1680.

Shu Wei, Dong-Xiao Lu, Jing Sun, Yan He, Longfeng Zhu, Yong-Lai Zhang, Feng-Shou Xiao. Solvothermal synthesis of highly porous polymers and their controllable transition from macro/mesoporosity to meso/microporosity. Colloids and Surfaces A: Physicochem. Eng. Aspects 414 (**2012**) 327–332.

Yamamoto, T.; Lee, B.-L. New Soluble, Coplanar Poly(naphthalene-2,6-diyl)-Type -Conjugated Polymer, Poly(pyrimido[5,4-d]pyrimidine-2,6-diyl), with Nitrogen Atoms at All of the o-Positions. Synthesis, Solid Structure, Optical Properties, Self-Assembling Phenomena, and Redox Behavior. *Macromolecules* **2002**, 35, 2993–2999.

Yang, JJ; Shi, RF; Zhou, P; Qiu, QM; Li, H. Asymmetric Schiff bases derived from diaminomaleonitrile and their metal complexes. J. Mol. Struc. 2016, 1106, 242-258.

C. Yang, B. Wang, L. Zhang, L. Yin, X. Wang, Angew. Chem. Int. Ed. **2017**, 56, 6627–6631.

P. Yang, R. Wang, M. Zhou and X. Wang, *Angew. Chem., Int. Ed.*, **2018**, 130, 8810–8813.

Zare, N; Zabardasti, A. A new nano-sized mononuclear Cu (II) complex with N,N-donor Schiff base ligands: sonochemical synthesis, characterization, molecular modeling and biological activity. App. Organomet. Chem. **2019**, 33, e4687.

Zhou, X.; Fang, Y.; Su, Y.; Ge, C.; Jin, B.; Li, Z.;Wu, S. Preparation and Characterization of Poly-Hydrogen Cyanide Nanofibers with High Visible Light Photocatalytic Activity. Catal. Commun. **2014**, 46, 197–200.

Encyclopedia of reagents for organic synthesis. (**2001**). Editorial Board: André Charette, Jeffrey Bode, Tomislav Rovis, and Ryan Shenvi. Wiley. Print ISBN: 9780471936237, Online ISBN: 9780470842898, DOI: 10.1002/047084289X.

Solvents and Solvent Effects in Organic Chemistry. Christian Reichardt and Thomas Welton. First published:27 October 2010. Print ISBN:9783527324736. Online ISBN:9783527632220. DOI:10.1002/9783527632220. Copyright © 2011 Wiley-VCH Verlag GmbH & Co. KGaA.